

Tiled Prompts: Overcoming Prompt Underspecification in Image and Video Super-Resolution

Bryan Sangwoo Kim ^{*1} Jonghyun Park ^{*1} Jong Chul Ye ¹

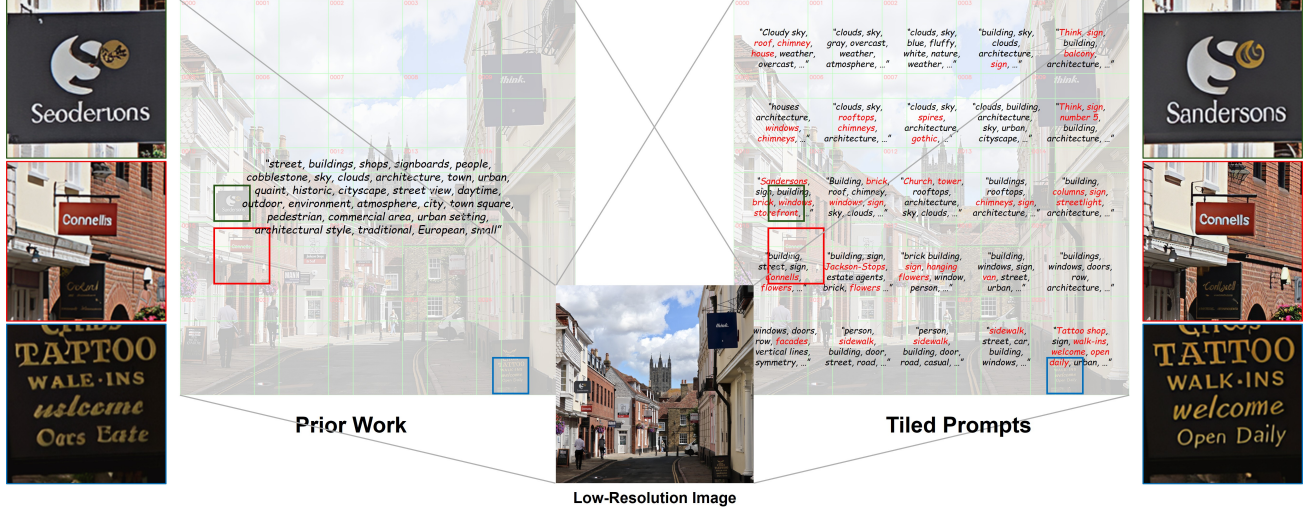


Figure 1. (Left) Relying on a single, global prompt for the latent tiling strategy during super-resolution causes *prompt underspecification*, leading to suboptimal reconstructions. (Right) Using *tiled prompts* solves ambiguity and provides accurate localized guidance needed to reconstruct high-quality details (e.g., text on signs are correctly generated only when their corresponding prompts are provided).

Abstract

Text-conditioned diffusion models have advanced image and video super-resolution by using prompts as semantic priors, but modern super-resolution pipelines typically rely on latent tiling to scale to high resolutions, where a single global caption causes *prompt underspecification*. A coarse global prompt often misses localized details (prompt sparsity) and provides locally irrelevant guidance (prompt misguidance) that can be amplified by classifier-free guidance. We propose Tiled Prompts, a unified framework for image and video super-resolution that generates a tile-specific prompt for each latent tile and performs super-resolution under locally text-conditioned posteriors, providing high-information guidance

^{*}Equal contribution ¹Graduate School of AI, Korea Advanced Institute of Science and Technology (KAIST), Daejeon, Republic of Korea. Correspondence to: Jong Chul Ye <jong.ye@kaist.ac.kr>.

Preprint. February 4, 2026.

that resolves prompt underspecification with minimal overhead. Experiments on high resolution real-world images and videos show consistent gains in perceptual quality and text alignment, while reducing hallucinations and tile-level artifacts relative to global-prompt baselines.

1. Introduction

Single Image Super-Resolution (SISR) aims to recover a high-resolution (HR) representation from a low-resolution (LR) input. As a fundamental low-level vision task, it is crucial for a wide range of applications, from enhancing legacy media to improving scientific visualization and medical imaging systems (Betzig et al., 2006; Oktay et al., 2016; Ravishankar & Bresler, 2010; Wang et al., 2022a). However, SISR is an ill-posed inverse problem; for any given LR input, there exists a multitude of plausible HR solutions. Modern deep learning approaches typically address this by learning the posterior probability distribution

$$p(\mathbf{x}_H \mid \mathbf{x}_L) \quad (1)$$

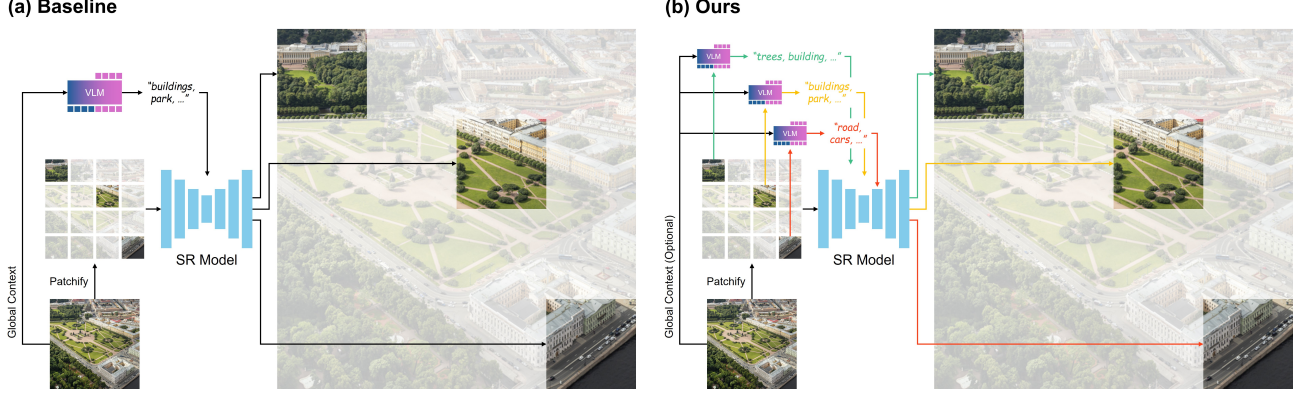


Figure 2. (a) Baseline Methods: Conditioning super-resolution models solely on a single global text prompt demonstrates the problem of prompt underspecification. The global prompt, while broadly describing the image, proves insufficient to constrain the fine-grained super-resolution process. **(b) Our Method (Tiled Prompts):** Our framework leverages dense, context-aware *tiled prompts* for each region. This localized textual guidance provides precise semantic anchors, enabling the super-resolution model to produce significantly sharper, more coherent, and perceptually richer details.

from large-scale datasets, where the LR input \mathbf{x}_L is mapped to its HR reconstruction \mathbf{x}_H . When properly trained, these models learn to effectively constrain the solution space, ensuring that the generated outputs are perceptually realistic.

Recent methods for super-resolution have significantly advanced this field by incorporating pre-trained generative models (*e.g.*, diffusion models), exploiting their rich generative priors for the super-resolution task (Wang et al., 2024; Wu et al., 2024b; Yu et al., 2024; Wu et al., 2024a). A key advantage of these generative frameworks is their ability to leverage textual conditioning. Since modern generative backbones are trained on diverse image-text pairs (Rombach et al., 2022; Esser et al., 2024), they naturally allow for text-guided generation. This effectively reformulates Eq. (1) by conditioning the posterior probability distribution on additional textual guidance as follows:

$$p(\mathbf{x}_H \mid \mathbf{x}_L, \mathbf{c}_{\text{global}}) \quad (2)$$

where $\mathbf{c}_{\text{global}}$ is a textual condition for providing global context about the input image. These textual priors are critical in creating high-frequency details and serving as powerful semantic anchors that guide the reconstruction toward plausible outcomes (Wu et al., 2024a; Kim et al., 2025).

This trend toward text-conditioned super-resolution extends naturally to Video Super-Resolution (VSR), currently an active area of research. Text-conditioned VSR can be expressed by simply replacing the image pair $\{\mathbf{x}_H, \mathbf{x}_L\}$ with a temporally dependent sequence pair $\{\mathbf{x}_H^{1:N}, \mathbf{x}_L^{1:N}\}$, which enables the joint super-resolution of the N frames comprising a video:

$$p(\mathbf{x}_H^{1:N} \mid \mathbf{x}_L^{1:N}, \mathbf{c}_{\text{global}}) \quad (3)$$

Analogous to SISR, text-conditioning for VSR is important for correct reconstruction of high-frequency details.

However, as interest in increasingly high-resolution imagery continues to grow, standard text-conditioning paradigms face a critical limitation. Modern super-resolution methods typically rely on a *latent tiling strategy* (Jiménez, 2023; Bar-Tal et al., 2023) of processing small, overlapping tiles rather than full-sized latents, to mitigate the roughly quadratic growth in VRAM usage as resolution scales. In this tiled regime, we encounter the problem of *prompt underspecification*: textual guidance derived from a single global caption $\mathbf{c}_{\text{global}}$ often lacks the specific, localized details needed to reconstruct individual tiles faithfully. At extreme resolutions (*e.g.*, 4K super-resolution), the number of tiles can easily reach on the order of hundreds. This semantic misalignment between the global prompt and local visual content inhibits the fine-grained textual guidance needed for plausible SR, a limitation that commonly arises in both SISR and VSR.

In this work, we propose *Tiled Prompts*: a unified framework to overcome text sparsity in image and video super-resolution. Rather than relying on a single, often irrelevant global prompt $\mathbf{c}_{\text{global}}$, our approach generates a dense, descriptive prompt $\mathbf{c}_{\text{local}}^{(i)}$ specific to each i -th tile. This reformulation effectively replaces Eq. (2) and Eq. (3) with a product of local posteriors¹:

$$\prod_{i=1}^N p_i \left(\mathbf{x}_H^{(i)} \mid \mathbf{x}_L^{(i)}, \mathbf{c}_{\text{local}}^{(i)} \right) \quad (4)$$

This local prompt provides high mutual information with the visual content of the tile, resolving prompt underspecification by giving the SR model the precise guidance it needs to reduce ambiguity and hallucination. Specifically,

¹For simplicity, we unify both image and video cases with the notations $\mathbf{x}_L \in \mathbb{R}^{T \times H \times W \times C}$ and $\mathbf{x}_H \in \mathbb{R}^{T \times rH \times rW \times C}$ for LR input and HR output respectively ($T = 1$ corresponds to SISR).

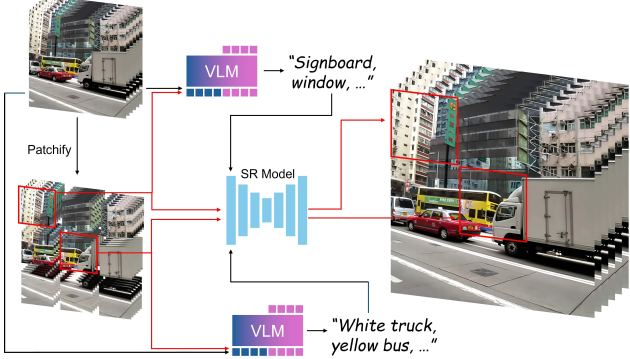


Figure 3. Our **Tiled Prompts** framework for VSR first divides the low-resolution video into a grid of spatio-temporal “tubes” or volumes, where each tube is a spatial patch that extends for the full duration of the video. A VLM then analyzes the local video content and generates a detailed text prompt that accurately describes the events within that patch. This localized prompt is then fed into the 3D VSR model to guide the reconstruction of that specific patch-volume, significantly improving textual guidance.

the proposed framework solves *prompt sparsity* by supplementing prompts that can be overlooked when generating a single global prompt (e.g., the red prompts in Fig. 1). Using tiled prompts also solves *prompt misguidance* that occurs due to irrelevance between a global prompt and local visual content. We show that the existence of irrelevant prompts cause off-target semantics to be amplified by Classifier-Free Guidance (CFG) (Ho & Salimans, 2022); thus, using tiled prompts improve both visual quality and text alignment of reconstructed images and videos.

The proposed framework is highly effective for alleviating prompt underspecification in both SISR and VSR. Though VSR shares the same fundamental goal as SISR, VSR demands the added challenge of enforcing consistency along an additional temporal axis. This added dimension significantly exacerbates the underspecification problem, thus making it even more inadequate for a single global prompt to be used to explain an entire video. We demonstrate that tiled prompts capture dynamic content, scene changes, and localized details that are otherwise overlooked, even while introducing minimal computational overhead.

Our contributions can be summarized as follows:

- We formally define the *prompt underspecification* problem found in the commonly used latent tiling strategy, and analyze its negative impacts for super-resolution.
- We introduce a unified framework to mitigate text sparsity that utilizes *tiled prompts* for localized textual guidance, presenting a viable solution for both SISR and VSR.

2. Related Work

2.1. Text-guided Image Super-Resolution

State-of-the-art models incorporate pre-trained generative models, and fine-tune their generative priors for super-resolution. During this process, textual priors are used to guide high frequency details of the super-resolution process. StableSR (Wang et al., 2024) employs a diffusion prior without any prompt, while SUPiR (Yu et al., 2024) trains the model with detailed text prompts to enrich semantic guidance. SeeSR (Wu et al., 2024b) introduces a Degradation-Aware Prompt Extractor (DAPE) that injects semantically rich prompts to encourage finer detail generation. OSEDiff (Wu et al., 2024a) and PiSA-SR (Sun et al., 2025a) further accelerate the SR process into a one-step denoising framework, while using text guidance for fine details. More recently, TeReDiff (Min et al., 2025) proposes Text-Aware Image Restoration (TAIR), which leverages explicit textual cues extracted from the image to faithfully recover text that is otherwise ambiguous in low-quality inputs.

As the role of textual guidance becomes increasingly prominent, the super-resolution community has begun to incorporate Vision-Language Models (VLMs) to leverage their visual understanding capabilities. Recent baselines such as SUPiR (Yu et al., 2024) and DiT4SR (Duan et al., 2025) use LLaVA (Liu et al., 2023) as a prompt extractor. Chain-of-Zoom (Kim et al., 2025) studies extreme super-resolution with VLMs, showing that scale autoregression, coupled with carefully structured text guidance, can progressively improve SR quality through iterative magnification. However, to the best of our knowledge, prior work has not explored using VLMs to provide effective guidance across the full spatial extent of high-resolution images during tiled SR inference. In this work, we address prompt underspecification by incorporating tile-level prompting via VLMs to supply localized guidance.

2.2. Video Super-Resolution

To fully exploit the generative capability of modern diffusion-based models, recent works have incorporated text-to-image (T2I) and text-to-video (T2V) priors into Video Super-Resolution (VSR). T2I-based VSR approaches suffer from temporal inconsistency, resulting in noticeable flickering artifacts across frames. To address this issue, Upscale-A-Video (Zhou et al., 2023) and MGLD-VSR (Yang et al., 2024) fine-tune pretrained T2I models by leveraging optical flow between adjacent frames. While effective to some extent, such fine-tuning compromises the diffusion model’s inherent image generation fidelity. To preserve generative quality while improving temporal stability, DLoRAL (Sun et al., 2025b) introduces a dual-LoRA framework that enhances temporal consistency without sacrificing generation ability, enabling efficient one-step VSR generation.

Another line of work directly leverages T2V priors for improved temporal coherence, instead of using T2I priors. While using T2V priors alleviates temporal inconsistency, naively adapting them to restoration degrades per-frame fidelity, especially under complex real-world degradations. To address this, STAR (Xie et al., 2025) augments large T2V backbones such as I2VGen-XL (Zhang et al., 2023) or CogVideoX (Yang et al., 2025) with a lightweight local-detail enhancement module to better preserve fine structures, along with a frequency-aware objective for improved fidelity. SeedVR (Wang et al., 2025b) proposes a scalable diffusion-transformer backbone for generic video restoration via (shifted) window attention, and SeedVR2 (Wang et al., 2025a) further advances this direction toward one-step video restoration through diffusion adversarial post-training. Stream-DiffVSR (Shiu et al., 2025) introduces a causally conditioned diffusion framework for low-latency online VSR that operates only on past frames. Despite their dependency on textual guidance for accurate reconstruction, none of these prior works fully validate the correctness of the prompts that are used. In this work, we introduce the problem of prompt underspecification, and solve it by providing tiled prompts in a localized manner.

3. Preliminaries

3.1. General Training Strategy for SR Models

Super-resolution (SR) is the task of sampling a high-resolution (HR) output $\mathbf{x}_H \in \mathbb{R}^{T \times rH \times rW \times C}$ given a low-resolution (LR) input $\mathbf{x}_L \in \mathbb{R}^{T \times H \times W \times C}$, for a given upscaling ratio r . Note that we unify cases for image ($T = 1$) and video ($T > 1$) through the notation above. Denoting the space of HR images as \mathcal{X}_{HR} and the space of LR images as \mathcal{X}_{LR} , we can train an SR model f_θ to learn the mapping:

$$f_\theta : \mathcal{X}_{\text{LR}} \rightarrow \mathcal{X}_{\text{HR}} \quad (5)$$

Training f_θ is nontrivial, as this mapping inherently ill-posed and highly complex. Thus, recent frameworks adapt large-scale T2I models for the SR task, incorporating text prompts \mathbf{c} as auxiliary conditions to effectively constrain the solution space. These models are typically trained on smaller crops of size $t \times k_1 \times k_2$, extracted from the training dataset $\mathcal{D}_{\text{train}}$, to optimize a composite objective function:

$$\min_{\theta} \mathbb{E}_{\substack{(\mathbf{x}_H, \mathbf{x}_L, \mathbf{c}) \sim \mathcal{D}_{\text{train}} \\ \hat{\mathbf{x}}_H \sim f_\theta(\hat{\mathbf{x}}_H | \mathbf{x}_L, \mathbf{c})}} [\mathcal{L}(\mathbf{x}_H, \hat{\mathbf{x}}_H)] \quad (6)$$

where \mathbf{c} is the text prompt. Depending on the framework, \mathcal{L} can consist of simple reconstruction terms (e.g., ℓ_1, ℓ_2), perceptual objectives (e.g., LPIPS, adversarial loss), or probabilistic objectives (e.g., denoising score matching). Regardless, the overall objective remains the same: to minimize the reconstruction error while leveraging \mathbf{c} to alleviate the ambiguity of the inverse problem.

3.2. Latent Tiling during Inference of SR Models

When input LR data exceeds the optimal processing size of the SR model, current methods split the input into a grid of tiles and perform SR at the tile-level to satisfy memory and compute constraints. This *latent tiling* strategy is not unique to super-resolution; it is widely used in high-resolution generative modeling (Jiménez, 2023; Bar-Tal et al., 2023), where overlapping tiles are processed independently and then merged to produce a full-resolution sample. For an LR tile of size $t \times k_1 \times k_2$, \mathbf{x}_L is split into a grid of tiles,

$$\left\{ \mathbf{x}_L^{(i)} \right\}_{i=1}^N, \quad \mathbf{x}_L^{(i)} \in \mathbb{R}^{t \times k_1 \times k_2 \times C} \quad (7)$$

where the LR tile $\mathbf{x}_L^{(i)}$ corresponds to an HR region $R^{(i)} \subset \{1, \dots, T\} \times \{1, \dots, rH\} \times \{1, \dots, rW\}$ of size $t \times (rk_1) \times (rk_2)$ at the scaled location. In practice, tiling is performed in the model’s latent space rather than directly in pixel space, but we retain the notation in Eq. (7) to denote these latent tiles for simplicity.

Given a global text condition $\mathbf{c}_{\text{global}}$, the text-conditioned SR model trained on the conditional probability distribution of Eq. (2) operates *per-tile* as follows:

$$\hat{\mathbf{x}}_H^{(i)} \sim f_\theta(\mathbf{x}_H^{(i)} | \mathbf{x}_L^{(i)}, \mathbf{c}_{\text{global}}) \quad (8)$$

where f_θ denotes the SR model with parameters θ . The resulting full HR output is the direct placement of predicted tiles onto their HR grid cells:

$$\hat{\mathbf{x}}_H(t, h, w) = \sum_{i=1}^N \mathbb{1}_{\{(t, h, w) \in R_i\}} \hat{\mathbf{x}}_H^{(i)}(\phi_i(t, h, w)) \quad (9)$$

where $\mathbb{1}_{\{(t, h, w) \in R_i\}}$ is the indicator for region R_i , and ϕ_i maps global HR coordinates $(t, h, w) \in R_i$ to local coordinates within tile i of size $t \times (rk_1) \times (rk_2)$. Equivalently, the global posterior is approximated as a product of disjoint tile-wise conditionals:

$$p(\mathbf{x}_H | \mathbf{x}_L, \mathbf{c}_{\text{global}}) \approx \prod_{i=1}^N p_i \left(\mathbf{x}_H^{(i)} | \mathbf{x}_L^{(i)}, \mathbf{c}_{\text{global}} \right) \quad (10)$$

where $\hat{\mathbf{x}}_H$ is obtained by the aggregation rule in Eq. 9.

In practice, direct aggregation often introduces boundary discontinuities, so a standard practice is to overlap tiles with Gaussian blending (Liang et al., 2021). Let $w_i(h, w) \geq 0$ be a Gaussian weighting window supported on R_i (and zero elsewhere). The aggregated HR estimate is then given by:

$$\hat{\mathbf{x}}_H(h, w) = \frac{\sum_{i=1}^N w_i(h, w) \hat{\mathbf{x}}_H^{(i)}(\phi_i(h, w))}{\sum_{i=1}^N w_i(h, w)} \quad (11)$$

In video SR, we adopt a valid region strategy: tiles are processed with overlap, but only the central valid region of each output tile is retained and boundary pixels are discarded, which reduces boundary artifacts.

4. Tiled Prompts

4.1. Prompt Underspecification

Existing text-conditioned SR pipelines typically extract a single global prompt $\mathbf{c}_{\text{global}}$ from the full LR input $\mathbf{x}_L \in \mathbb{R}^{T \times H \times W \times C}$ and reuse it for all local tiles $\mathbf{x}_L^{(i)}$:

$$\hat{\mathbf{x}}_H^{(i)} \sim f_\theta(\mathbf{x}_H^{(i)} \mid \mathbf{x}_L^{(i)}, \mathbf{c}_{\text{global}}). \quad (12)$$

While $\mathbf{c}_{\text{global}}$ captures the overall scene context, it acts as a coarse constraint when applied to local tiles. Thus, tile-specific attributes are often omitted in the global prompt, while irrelevant details that do not appear in the i -th tile are included, leading to two main issues of prompt underspecification: (i) sparsity and (ii) misguidance.

Prompt Sparsity. During tiling-based SR, the text-conditioned posterior for tile i is modeled as

$$p(\mathbf{x}_H^{(i)} \mid \mathbf{x}_L^{(i)}, \mathbf{c}_{\text{global}}). \quad (13)$$

In Eq. (13) the same global context $\mathbf{c}_{\text{global}}$ is given for *all* tiles i , regardless of whether the content inside the local tile is actually described by the prompt $\mathbf{c}_{\text{global}}$. This problem of *prompt sparsity* occurs when $\mathbf{c}_{\text{global}}$ carries negligible incremental information about $\mathbf{x}_H^{(i)}$ once $\mathbf{x}_L^{(i)}$ is known. This can be formally defined as follows:

$$I\left(\mathbf{x}_H^{(i)}; \mathbf{c}_{\text{global}} \mid \mathbf{x}_L^{(i)}\right) \approx 0. \quad (14)$$

Equivalently, the conditional distribution degenerates to:

$$p(\mathbf{x}_H^{(i)} \mid \mathbf{x}_L^{(i)}, \mathbf{c}_{\text{global}}) \approx p(\mathbf{x}_H^{(i)} \mid \mathbf{x}_L^{(i)}). \quad (15)$$

Intuitively, $\mathbf{c}_{\text{global}}$ is too coarse to resolve the tile-level ambiguity. This sparsity causes the SR model to hallucinate or guess fine details, especially at high resolutions or temporally long videos. For example, Fig. 1 shows how the inclusion of certain prompts (e.g., “Sandersons”, “Connells”) is critical for the accurate reconstruction of text on signs; such text is often overlooked when incorporating only a single global prompt.

Prompt Misguidance. Modern text-conditioned SR methods are implemented as conditional diffusion models, often by adapting pretrained T2I or T2V diffusion backbones to the SR setting. Accordingly, they inherit Classifier-Free Guidance (CFG) (Ho & Salimans, 2022) as a standard inference mechanism to increase adherence to the text condition without modifying model parameters.

CFG amplifies the text conditioning signal by extrapolating the model prediction \mathbf{e} (e.g., noise ϵ or velocity \mathbf{v}):

$$\tilde{\mathbf{e}} = \mathbf{e}_{\text{uncond}} + s \cdot (\mathbf{e}_{\text{cond}} - \mathbf{e}_{\text{uncond}}). \quad (16)$$

Algorithm 1 Tiled Inference with Tiled Prompts

```

1: Require: LR Input  $\mathbf{x}_L$ , SR Model  $f_\theta$ , VLM  $Y_{\text{VLM}}$ , crop size  $(t, k_1, k_2)$ , overlap parameters, scale  $r$ , timesteps  $\{\tau_m\}_{m=1}^T$ , scheduler  $\mathcal{S}$ 
2: Compute tiling coordinates  $\{R_i\}_{i=1}^N$ 
3: for  $i = 1 \rightarrow N$  do
4:    $\mathbf{x}_L^{(i)} \leftarrow \text{Crop}(\mathbf{x}_L, R_i)$ 
5:    $\mathbf{c}_{\text{local}}^{(i)} \sim Y_{\text{VLM}}(\mathbf{x}_L^{(i)}; \eta_i)$  ▷ Tiled Prompts
6: end for
7: Compute Gaussian window  $w_i$  for region  $R_i$ 
8: Initialize  $\mathbf{z}^{(T)} \leftarrow \text{InitNoise}()$ 
9: for  $m = T \rightarrow 1$  do
10:   for  $i = 1 \rightarrow N$  do
11:      $\mathbf{z}^{(i,m)} \leftarrow \text{Crop}(\mathbf{z}^{(m)}, R_i)$  ▷ Tiled Inference
12:      $\hat{\mathbf{e}}^{(i)} \leftarrow f_\theta(\mathbf{z}^{(i,m)}, \mathbf{x}_L^{(i)}, \mathbf{c}_{\text{local}}^{(i)}, \tau_m)$ 
13:      $\mathbf{E}(R_i) \leftarrow \mathbf{E}(R_i) + w_i \cdot \hat{\mathbf{e}}^{(i)}$  ▷ Aggregation
14:      $\mathbf{W}(R_i) \leftarrow \mathbf{W}(R_i) + w_i$ 
15:   end for
16:    $\hat{\mathbf{e}} \leftarrow \mathbf{E} \oslash \mathbf{W}$  ▷ Normalization
17:    $\mathbf{z}^{(m-1)} \leftarrow \mathcal{S}(\mathbf{z}^{(m)}, \hat{\mathbf{e}}, \tau_m)$ 
18: end for
19:  $\mathbf{x}_H \leftarrow \text{Decode}(\mathbf{z}^{(0)})$ 
20: return  $\mathbf{x}_H$ 

```

where $s > 1$ is the guidance scale. The key term is the guidance direction $\Delta \mathbf{e} := \mathbf{e}_{\text{cond}} - \mathbf{e}_{\text{uncond}}$, which biases the denoising trajectory toward semantics implied by the given text. When the global prompt $\mathbf{c}_{\text{global}}$ contains semantics that are irrelevant or contradictory to the local visual content of a tile, $\Delta \mathbf{e}$ for a given tile becomes misaligned with the tile’s correct denoising direction. Let

$$\Delta \mathbf{e}_i(\mathbf{c}_{\text{global}}) := \mathbf{e}_{\text{cond}} - \mathbf{e}_{\text{uncond}} \quad (17)$$

denote the CFG guidance direction for tile i under text condition $\mathbf{c}_{\text{global}}$, and decompose

$$\Delta \mathbf{e}_i(\mathbf{c}_{\text{global}}) = \Delta \mathbf{e}_i^* + \delta_i(\mathbf{c}_{\text{global}}) \quad (18)$$

into an ideal direction $\Delta \mathbf{e}_i^*$ and an error term $\delta_i(\mathbf{c}_{\text{global}})$. CFG scales this error by the guidance scale s ,

$$\tilde{\mathbf{e}}_i(\mathbf{c}_{\text{global}}) = \mathbf{e}_{\text{uncond}} + s \Delta \mathbf{e}_i^* + s \delta_i(\mathbf{c}_{\text{global}}), \quad (19)$$

and the error compounds across denoising steps. We define the term $\|\delta_i(\mathbf{c}_{\text{global}})\|$ as *prompt misguidance*, which pushes the SR output toward an incorrect semantic mode and produces artifacts. For example, in Fig. 1 the global prompt contains irrelevant information describing other regions (e.g., “sky” is used for guiding streets and buildings). Such prompt misguidance perturbs the estimated score (or velocity) in a direction inconsistent with the local conditional posterior.



Figure 4. Qualitative results for image super-resolution. (a,b) **Input**: The low-resolution input and a cropped tile to be upsampled. (c) **SR with Global Prompt**: The baseline result using only a single, coarse global prompt. As the text prompt does not provide sufficient guidance, super-resolution results are inaccurate. (d) **SR with Tiled Prompt (Ours)**: Our method uses dense, localized textual guidance to generate significantly more accurate and semantically plausible high-frequency details consistent with the context.

4.2. Tiled Prompts for Image SR

To address prompt underspecification under tiled inference, we introduce *Tiled Prompts*, which replaces the single global prompt with *tile-specific* textual conditions. Specifically, instead of broadcasting a single caption c_{global} to all tiles as in Fig. 2(a), we extract local prompts using a VLM conditioned on each local tile as in Fig. 2(b). This allows for dense, localized guidance that is better aligned with the visual evidence within each tile.

For each LR tile $\mathbf{x}_L^{(i)}$, we generate a corresponding local prompt by leveraging a VLM as a prompt extractor:

$$c_{\text{local}}^{(i)} := Y_{\text{VLM}}(\mathbf{x}_L^{(i)}; \eta_i) \quad (20)$$

where η_i is sampling noise. The tile-wise prompt $c_{\text{local}}^{(i)}$ is then used as the text condition for super-resolution:

$$\hat{\mathbf{x}}_H^{(i)} \sim f_{\theta}(\mathbf{x}_H^{(i)} | \mathbf{x}_L^{(i)}, c_{\text{local}}^{(i)}). \quad (21)$$

Accordingly, the global conditional distribution under tiled inference is approximated by the product of conditionals,

$$p(\mathbf{x}_H | \mathbf{x}_L, \{c_{\text{local}}^{(j)}\}_{j=1}^N) \approx \prod_{i=1}^N p_i(\mathbf{x}_H^{(i)} | \mathbf{x}_L^{(i)}, c_{\text{local}}^{(i)}), \quad (22)$$

with aggregation performed as in Sec. 3.2. A detailed description of the procedure is given in Algorithm 1.

Collectively, the set of local prompts $\{c_{\text{local}}^{(j)}\}_{j=1}^N$ effectively mitigates both prompt sparsity and misguidance by providing localized, tile-specific semantics that are typically absent or misleading in a single global caption. Tiled prompts reduce the misguidance $\|\delta_i(c)\|$ by constructing $c = c_{\text{local}}^{(i)}$ to be semantically consistent with the tile, thereby improving fidelity and reducing artifacts at high resolutions.

4.3. Tiled Prompts for Video SR

The prompt underspecification described in Sec. 4.1 is exacerbated in Video Super Resolution (VSR), where the LR input $\mathbf{x}_L \in \mathbb{R}^{T \times H \times W \times C}$ forms a spatio-temporal volume. Nonetheless, standard text-conditioned VSR pipelines often condition the entire sequence on a single static global prompt c_{global} . This yields a *dual sparsity* effect: *spatial sparsity*, where c_{global} omits spatial details as for the image case, and *temporal sparsity*, where c_{global} lacks the temporal granularity needed to describe local dynamics (e.g., motion, evolution) within each tile volume.

Context-assisted Tiled Prompts. A direct extension of our image setting would be to extract a prompt from each local tile volume alone. However, in practice, VLMs struggle to infer accurate motion level descriptions from a small cropped spatio-temporal window. In accordance with the amplified underspecification, we provide the prompt-extraction VLM with additional global context from the full LR sequence \mathbf{x}_L to generate our tiled prompts:

$$c_{\text{local}}^{(i)} := Y_{\text{VLM}}(\mathbf{x}_L^{(i)}, \mathbf{x}_L; \eta_i), \quad (23)$$

where η_i denotes sampling noise. Although the global input \mathbf{x}_L is shared across tiles, the output $c_{\text{local}}^{(i)}$ remains tile specific because it is anchored to the local evidence in $\mathbf{x}_L^{(i)}$. Furthermore, we provide explicit instructions through system prompts and user prompts to account for the additional global context and fully leverage the reasoning capability of the VLM. The global context aware prompt $c_{\text{local}}^{(i)}$ encodes localized dynamics (e.g., “spinning wheels” instead of only “car”), thereby mitigating both spatial and temporal sparsity. The tile-wise prompt $c_{\text{local}}^{(i)}$ is then substituted into Eq. (21) for tiled inference and aggregation.

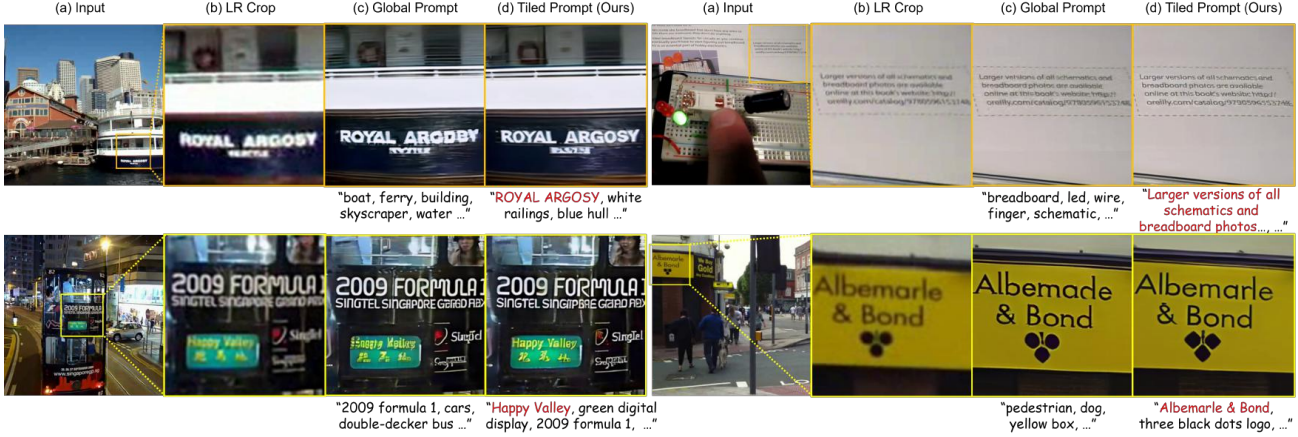


Figure 5. Qualitative results for video super-resolution. (a,b) **Input**: A low-resolution input frame and its cropped tile before SR. (c) **SR with Global Prompt**: Using only a coarse global prompt does not provide sufficient guidance, causing inaccurate SR results. (d) **SR with Tiled Prompt (Ours)**: Our method of using dense, localized textual guidance proves effectively reconstructs details in videos.

Table 1. Quantitative comparison on image quality metrics and image-text alignment metrics. Best.

Dataset	Prompt Type	Image Quality				Image-Text Alignment		
		NIQE↓	MUSIQ↑	MANIQA↑	CLIPQA↑	CLIP Score↑	ImageReward↑	HPSv2↑
LSDIR1K	Global (Baseline)	2.9427	63.8677	0.6373	0.6886	25.5731	-1.6030	0.1739
	Global + Local	2.9418	64.0749	0.6379	0.6932	26.0911	-1.4717	0.1864
	Local	2.9040	63.9731	0.6350	0.6917	27.5817	-0.5404	0.2141
URBAN100	Global (Baseline)	3.6156	53.1372	0.6668	0.6715	26.0509	-1.2786	0.1885
	Global + Local	3.5724	53.8299	0.6681	0.6784	26.4038	-1.1231	0.2006
	Local	3.5001	54.9203	0.6618	0.6780	27.7176	-0.4936	0.2188
OST300	Global (Baseline)	2.9547	66.3813	0.6536	0.6799	25.2165	-1.8551	0.1609
	Global + Local	2.9455	66.8685	0.6555	0.6875	25.6453	-1.8244	0.1732
	Local	2.9007	66.7233	0.6518	0.6943	27.0687	-0.7806	0.2070

5. Experiments

5.1. Experimental Settings

Image Experiments. We use DiT4SR (Duan et al., 2025) as our base SR model, a recent model that uses a diffusion transformer as its generative backbone. Global and local (tiled) prompts are extracted with Qwen2.5-VL-7B-Instruct (Team, 2025a).

We evaluate our framework on the real-world datasets Urban100 (Huang et al., 2015), OST300 (Wang et al., 2018), and the first 1K images from LSDIR (Li et al., 2023) which we term LSDIR1K. We do not use common low-resolution datasets such as DrealSR (Wei et al., 2020), RealSR (Cai et al., 2019), RealLR200 (Wu et al., 2024b), or RealLQ250 (Ai et al., 2024), as we find their low resolutions inappropriate for validating the latent tiling performance. Each image is resized and cropped to a resolution of 512×512 , producing a resolution of 2048×2048 after $4 \times$ magnification. During tiled inference, each LR latent is divided into tiles of size 64×64 with an overlap of 16, resulting in 25 tiles total.

Video Experiments. For video experiments, we use the pretrained video SR model STAR (Xie et al., 2025) based on the I2VGen-XL backbone (Zhang et al., 2023), which

is widely used and publicly available with text-conditioned training. Global and local (tiled) prompts are extracted using Qwen3-VL-8B-Instruct (Team, 2025b), which possesses improved spatio-temporal understanding.

We evaluate our framework on the real-world datasets VideoLQ (Chan et al., 2021), RealVSR (YANG et al., 2021), and MVSR4x (Wang et al., 2022b). Unlike the image experiments, we do not apply spatial resizing or cropping, and directly process the entire video sequences as inputs. As STAR operates in a video-to-video refinement manner, all low-resolution inputs are first upsampled by $4 \times$ using bicubic interpolation and then divided into spatio-temporal volumes of size $32 \times 720 \times 1280$ for tiled inference.

5.2. Comparison Results for Image SR

We evaluate the performance of our framework regarding overall image quality and image-text alignment in Tab. 1. As no dataset provides ground-truth images of 2048×2048 resolution for reference-based comparison, we rely on no-reference metrics to assess the perceptual quality of images: NIQE (Zhang et al., 2015), MUSIQ (Ke et al., 2021), MANIQA (Yang et al., 2022), CLIPQA (Wang et al., 2023). Results show that providing tiled (local) prompts as additional guidance consistently improves image quality com-

Table 2. Quantitative comparison on frame-wise quality, video quality, and video-text alignment metrics. **Best**, Second-Best.

Dataset	Prompt Type	Frame-wise Quality			Video Quality			Video-Text Alignment			
		NIQE \downarrow	MUSIQ \uparrow	MANIQA \uparrow	CLIP-IQA \uparrow	HYPER-IQA \uparrow	Faster VQA \uparrow	FAST-VQA \uparrow	DOVER \uparrow	Language Bind \uparrow	VQA (LLAQA) \uparrow
VideoLQ	Global (Baseline)	4.7039	45.1177	0.4788	0.2599	0.3923	0.7393	0.7501	53.6491	0.4260	0.1914
	Global + Local	4.6610	45.6111	0.4833	0.2602	0.3952	0.7461	0.7524	54.0278	0.4839	0.1959
	Local	4.5221	46.8296	0.4938	0.2637	0.4087	0.7526	0.7640	54.6805	0.6004	0.2023
RealVSR	Global (Baseline)	4.0802	69.6148	0.6741	0.3179	0.5759	0.7421	0.7282	53.3358	0.1227	0.0584
	Global + Local	4.0803	69.6222	0.6752	0.3180	0.5760	0.7454	0.7289	53.3789	0.5897	0.1258
	Local	4.0694	70.6310	0.6831	0.3293	0.5890	0.7499	0.7255	53.7794	0.7467	0.2272
MVSF	Global (Baseline)	6.1917	36.3630	0.3541	0.2366	0.3598	0.4480	0.4118	19.3979	0.0442	0.0450
	Global + Local	6.1707	36.4164	0.3525	0.2358	0.3588	0.4981	0.4217	19.5745	0.6093	0.1403
	Local	5.9709	36.0415	0.3567	0.2377	0.3642	0.4982	0.4366	19.9026	0.6556	0.1719

Table 3. Inference time with latent tiling (seconds). The number inside parentheses denote the number of tiles.

Method	Time	Method	Time
DiT4SR + Tiled Prompts (25)	162.58 166.15	STAR + Tiled Prompts (12)	1266.1 1341.6

pared to the baseline of using a single global prompt.

To validate that our framework alleviates prompt underspecification, we measure image-text alignment between each image tile and the corresponding text prompt used for guidance. These metrics quantify the relevance of the conditioning text to the local visual content during SR. We use the metrics CLIPS (Hessel et al., 2021), ImageReward (Xu et al., 2024), and HPSv2 (Wu et al., 2023b) to assess this correspondence. The baseline scenario used for comparison uses a single global text prompt (from a global extractor) for all tiles, while our method uses localized prompts for each tile. Our framework shows significant increase in alignment between local content and textual description, showing that incorporating tiled prompts into tiled inference endues more accurate and meaningful guidance. These results are further supported by qualitative comparison provided in Fig. 4.

5.3. Comparison Results for Video SR

We evaluate video restoration quality and video-text alignment in Tab. 2. Beyond frame-wise image metrics (*i.e.*, NIQE, MUSIQ, MANIQA, CLIP, HPSv2 (Su et al., 2020)), we employ video-specific metrics to assess temporal consistency and authentic video quality: Faster-VQA (Wu et al., 2022b), FAST-VQA (Wu et al., 2022a), and DOVER (Wu et al., 2023a) (focusing on video clarity).

As shown in Tab. 2, incorporating local (tiled) prompts consistently improves perceptual quality across all datasets. Notably, using strictly local prompts yields the best overall performance. The consistent gains in video-level metrics indicate that our dense, dynamic prompts help the model resolve motion ambiguity better than a static global prompt, resulting in enhanced spatio-temporal fidelity.

To assess whether local prompting mitigates prompt underspecification in videos, we measure semantic alignment

between each spatio-temporal tile and its corresponding text prompt. We use LanguageBind (Zhu et al., 2024) and a VLM-based VQA evaluation protocol, following prior work (Lin et al., 2024), with LLaVA-OneVision (Li et al., 2024) as the evaluator. Substantial gains in text-video alignment are observed when using local prompts compared to using only a global prompt, confirming that tile-specific prompts provide accurate semantic guidance that aligns with local temporal dynamics. These results are further supported by qualitative comparison provided in Fig. 5.

5.4. Runtime Analysis

Tab. 3 shows that the additional computation introduced by our framework incurs negligible overhead relative to the overall super-resolution inference cost. Consequently, the observed improvements in image and video quality justify the extra computation, making the trade-off favorable.

6. Conclusion

We identified *prompt underspecification* as a key failure mode of text-conditioned super-resolution under the widely used latent tiling strategy, where a single global prompt is both too coarse to resolve tile-level ambiguity and prone to injecting irrelevant semantics that are amplified by CFG. To address this, we proposed *Tiled Prompts*, which replaces global text conditioning with tile-specific prompts to provide localized guidance for each latent tile. Across both SISR and VSR, tiled prompts improve perceptual quality and image/video-text alignment while introducing negligible computational overhead, offering a practical and unified solution for SR at high resolutions.

Limitations. Our framework’s reliance on multiple VLM forward passes makes it computationally more expensive than methods using only a single global prompt, though Tab. 3 shows that overhead is minimal. Furthermore, VLMs can misinterpret local content or hallucinate details; thus, an important direction for future work is to improve the robustness and reliability of VLM-based prompt extraction.

Impact Statement

This paper presents work whose goal is to advance the field of Machine Learning. There are many potential societal consequences of our work, none which we feel must be specifically highlighted here.

References

Ai, Y., Zhou, X., Huang, H., Han, X., Chen, Z., You, Q., and Yang, H. Dreamclear: High-capacity real-world image restoration with privacy-safe dataset curation. *Advances in Neural Information Processing Systems*, 37:55443–55469, 2024.

Bar-Tal, O., Yariv, L., Lipman, Y., and Dekel, T. Multi-diffusion: Fusing diffusion paths for controlled image generation, 2023. URL <https://arxiv.org/abs/2302.08113>.

Betzig, E., Patterson, G. H., Sougrat, R., Lindwasser, O. W., Olenych, S., Bonifacino, J. S., Davidson, M. W., Lippincott-Schwartz, J., and Hess, H. F. Imaging intracellular fluorescent proteins at nanometer resolution. *science*, 313(5793):1642–1645, 2006.

Cai, J., Zeng, H., Yong, H., Cao, Z., and Zhang, L. Toward real-world single image super-resolution: A new benchmark and a new model. In *Proceedings of the IEEE/CVF international conference on computer vision*, pp. 3086–3095, 2019.

Chan, K. C. K., Zhou, S., Xu, X., and Loy, C. C. Investigating tradeoffs in real-world video super-resolution, 2021.

Duan, Z.-P., Zhang, J., Jin, X., Zhang, Z., Xiong, Z., Zou, D., Ren, J. S., Guo, C., and Li, C. Dit4sr: Taming diffusion transformer for real-world image super-resolution. In *Proceedings of the IEEE/CVF International Conference on Computer Vision*, pp. 18948–18958, 2025.

Esser, P., Kulal, S., Blattmann, A., Entezari, R., Müller, J., Saini, H., Levi, Y., Lorenz, D., Sauer, A., Boesel, F., et al. Scaling rectified flow transformers for high-resolution image synthesis. In *Forty-first International Conference on Machine Learning*, 2024.

Hessel, J., Holtzman, A., Forbes, M., Le Bras, R., and Choi, Y. Clipscore: A reference-free evaluation metric for image captioning. In *Proceedings of the 2021 conference on empirical methods in natural language processing*, pp. 7514–7528, 2021.

Ho, J. and Salimans, T. Classifier-free diffusion guidance. *arXiv preprint arXiv:2207.12598*, 2022.

Huang, J.-B., Singh, A., and Ahuja, N. Single image super-resolution from transformed self-exemplars. In *Proceedings of the IEEE conference on computer vision and pattern recognition*, pp. 5197–5206, 2015.

Jiménez, Á. B. Mixture of diffusers for scene composition and high resolution image generation. *arXiv preprint arXiv:2302.02412*, 2023.

Ke, J., Wang, Q., Wang, Y., Milanfar, P., and Yang, F. Musiq: Multi-scale image quality transformer. In *Proceedings of the IEEE/CVF international conference on computer vision*, pp. 5148–5157, 2021.

Kim, B. S., Kim, J., and Ye, J. C. Chain-of-zoom: Extreme super-resolution via scale autoregression and preference alignment. *arXiv preprint arXiv:2505.18600*, 2025.

Li, B., Zhang, Y., Guo, D., Zhang, R., Li, F., Zhang, H., Zhang, K., Li, Y., Liu, Z., and Li, C. Llava-onevision: Easy visual task transfer. 2024. URL <https://arxiv.org/abs/2408.03326>.

Li, Y., Zhang, K., Liang, J., Cao, J., Liu, C., Gong, R., Zhang, Y., Tang, H., Liu, Y., Demandolx, D., et al. Lsdir: A large scale dataset for image restoration. In *Proceedings of the IEEE/CVF Conference on Computer Vision and Pattern Recognition*, pp. 1775–1787, 2023.

Liang, J., Cao, J., Sun, G., Zhang, K., Van Gool, L., and Timofte, R. Swinir: Image restoration using swin transformer. In *Proceedings of the IEEE/CVF International Conference on Computer Vision*, pp. 1833–1844, 2021.

Lin, Z., Pathak, D., Li, B., Li, J., Xia, X., Neubig, G., Zhang, P., and Ramanan, D. Evaluating text-to-visual generation with image-to-text generation. 2024. URL <https://arxiv.org/abs/2404.01291>.

Liu, H., Li, C., Wu, Q., and Lee, Y. J. Visual instruction tuning. *Advances in neural information processing systems*, 36:34892–34916, 2023.

Min, J., Kim, J. H., Cho, P. H., Lee, J., Park, J., Park, M., Kim, S., Park, H., and Kim, S. Text-aware image restoration with diffusion models, 2025. URL <https://arxiv.org/abs/2506.09993>.

Oktay, O., Bai, W., Lee, M., Guerrero, R., Kamnitsas, K., Caballero, J., de Marvao, A., Cook, S., O'Regan, D., and Rueckert, D. Multi-input cardiac image super-resolution using convolutional neural networks. In *Medical Image Computing and Computer-Assisted Intervention-MICCAI 2016: 19th International Conference, Athens, Greece, October 17-21, 2016, Proceedings, Part III 19*, pp. 246–254. Springer, 2016.

Ravishankar, S. and Bresler, Y. MR image reconstruction from highly undersampled k-space data by dictionary learning. *IEEE transactions on medical imaging*, 30(5):1028–1041, 2010.

Rombach, R., Blattmann, A., Lorenz, D., Esser, P., and Ommer, B. High-resolution image synthesis with latent diffusion models. In *Proceedings of the IEEE/CVF Conference on Computer Vision and Pattern Recognition*, pp. 10684–10695, 2022.

Shiu, H.-S., Lin, C.-Y., Wang, Z., Hsiao, C.-W., Yu, P.-F., Chen, Y.-C., and Liu, Y.-L. Stream-diffvsr: Low-latency streamable video super-resolution via auto-regressive diffusion, 2025.

Su, S., Yan, Q., Zhu, Y., Zhang, C., Ge, X., Sun, J., and Zhang, Y. Blindly assess image quality in the wild guided by a self-adaptive hyper network. In *Proceedings of the IEEE/CVF conference on computer vision and pattern recognition*, pp. 3667–3676, 2020.

Sun, L., Wu, R., Ma, Z., Liu, S., Yi, Q., and Zhang, L. Pixel-level and semantic-level adjustable super-resolution: A dual-lora approach. In *Proceedings of the Computer Vision and Pattern Recognition Conference*, pp. 2333–2343, 2025a.

Sun, Y., Sun, L., Liu, S., Wu, R., Zhang, Z., and Zhang, L. One-step diffusion for detail-rich and temporally consistent video super-resolution. In *The Thirty-ninth Annual Conference on Neural Information Processing Systems*, 2025b.

Team, Q. Qwen2.5-v1, January 2025a. URL <https://qwenlm.github.io/blog/qwen2.5-v1/>.

Team, Q. Qwen3 technical report, 2025b. URL <https://arxiv.org/abs/2505.09388>.

Wang, J., Chan, K. C., and Loy, C. C. Exploring clip for assessing the look and feel of images. In *Proceedings of the AAAI conference on artificial intelligence*, volume 37, pp. 2555–2563, 2023.

Wang, J., Yue, Z., Zhou, S., Chan, K. C., and Loy, C. C. Exploiting diffusion prior for real-world image super-resolution. *International Journal of Computer Vision*, 132(12):5929–5949, 2024.

Wang, J., Lin, S., Lin, Z., Ren, Y., Wei, M., Yue, Z., Zhou, S., Chen, H., Zhao, Y., Yang, C., Xiao, X., Loy, C. C., and Jiang, L. Seedvr2: One-step video restoration via diffusion adversarial post-training, 2025a.

Wang, J., Lin, Z., Wei, M., Zhao, Y., Yang, C., Loy, C. C., and Jiang, L. Seedvr: Seeding infinity in diffusion transformer towards generic video restoration. In *Proceedings of the Computer Vision and Pattern Recognition Conference*, 2025b.

Wang, P., Bayram, B., and Sertel, E. A comprehensive review on deep learning based remote sensing image super-resolution methods. *Earth-Science Reviews*, 232:104110, 2022a.

Wang, R., Liu, X., Zhang, Z., Wu, X., Feng, C.-M., Zhang, L., and Zuo, W. Benchmark dataset and effective inter-frame alignment for real-world video super-resolution. 2022b.

Wang, X., Yu, K., Dong, C., and Loy, C. C. Recovering realistic texture in image super-resolution by deep spatial feature transform. In *Proceedings of the IEEE conference on computer vision and pattern recognition*, pp. 606–615, 2018.

Wei, P., Xie, Z., Lu, H., Zhan, Z., Ye, Q., Zuo, W., and Lin, L. Component divide-and-conquer for real-world image super-resolution. In *European conference on computer vision*, pp. 101–117. Springer, 2020.

Wu, H., Chen, C., Hou, J., Liao, L., Wang, A., Sun, W., Yan, Q., and Lin, W. Fast-vqa: Efficient end-to-end video quality assessment with fragment sampling. In *Proceedings of the European conference on computer vision (ECCV)*, 2022a. URL <https://arxiv.org/abs/2207.02595>.

Wu, H., Chen, C., Liao, L., Hou, J., Sun, W., Yan, Q., Gu, J., and Lin, W. Neighbourhood representative sampling for efficient end-to-end video quality assessment. 2022b. URL <https://arxiv.org/abs/2210.05357>.

Wu, H., Zhang, E., Liao, L., Chen, C., Hou, J., Wang, A., Sun, W., Yan, Q., and Lin, W. Exploring video quality assessment on user generated contents from aesthetic and technical perspectives. In *Proceedings of the IEEE/CVF International Conference on Computer Vision (ICCV)*, 2023a. URL <https://arxiv.org/abs/2211.04894>.

Wu, R., Sun, L., Ma, Z., and Zhang, L. One-step effective diffusion network for real-world image super-resolution. *Advances in Neural Information Processing Systems*, 37:92529–92553, 2024a.

Wu, R., Yang, T., Sun, L., Zhang, Z., Li, S., and Zhang, L. Seesr: Towards semantics-aware real-world image super-resolution. In *Proceedings of the IEEE/CVF conference on computer vision and pattern recognition*, pp. 25456–25467, 2024b.

Wu, X., Hao, Y., Sun, K., Chen, Y., Zhu, F., Zhao, R., and Li, H. Human preference score v2: A solid benchmark for evaluating human preferences of text-to-image synthesis. *arXiv preprint arXiv:2306.09341*, 2023b.

Xie, R., Liu, Y., Zhou, P., Zhao, C., Zhou, J., Zhang, K., Zhang, Z., Yang, J., Yang, Z., and Tai, Y. Star: Spatial-temporal augmentation with text-to-video models for real-world video super-resolution. In *Proceedings of the IEEE/CVF International Conference on Computer Vision (ICCV)*, 2025.

Xu, J., Liu, X., Wu, Y., Tong, Y., Li, Q., Ding, M., Tang, J., and Dong, Y. Imagereward: Learning and evaluating human preferences for text-to-image generation. *Advances in Neural Information Processing Systems*, 36, 2024.

Yang, S., Wu, T., Shi, S., Lao, S., Gong, Y., Cao, M., Wang, J., and Yang, Y. Maniqa: Multi-dimension attention network for no-reference image quality assessment. In *Proceedings of the IEEE/CVF conference on computer vision and pattern recognition*, pp. 1191–1200, 2022.

YANG, X., Xiang, W., Zeng, H., and Zhang, L. Real-world video super-resolution: A benchmark dataset and a decomposition based learning scheme. 2021.

Yang, X., He, C., Ma, J., and Zhang, L. Motion-guided latent diffusion for temporally consistent real-world video super-resolution. In *Proceedings of the European conference on computer vision (ECCV)*, 2024.

Yang, Z., Teng, J., Zheng, W., Ding, M., Huang, S., Xu, J., Yang, Y., Hong, W., Zhang, X., Feng, G., Yin, D., Zhang, Y., Wang, W., Cheng, Y., Xu, B., Gu, X., Dong, Y., and Tang, J. Cogvideox: Text-to-video diffusion models with an expert transformer. In *International Conference on Learning Representations*, 2025.

Yu, F., Gu, J., Li, Z., Hu, J., Kong, X., Wang, X., He, J., Qiao, Y., and Dong, C. Scaling up to excellence: Practicing model scaling for photo-realistic image restoration in the wild. In *Proceedings of the IEEE/CVF Conference on Computer Vision and Pattern Recognition*, pp. 25669–25680, 2024.

Zhang, L., Zhang, L., and Bovik, A. C. A feature-enriched completely blind image quality evaluator. *IEEE Transactions on Image Processing*, 24(8):2579–2591, 2015.

Zhang, S., Wang, J., Zhang, Y., Zhao, K., Yuan, H., Qing, Z., Wang, X., Zhao, D., and Zhou, J. I2vgen-xl: High-quality image-to-video synthesis via cascaded diffusion models. 2023.

Zhou, S., Yang, P., Wang, J., Luo, Y., and Loy, C. C. Upscale-a-video: Temporal-consistent diffusion model for real-world video super-resolution. 2023.

Zhu, B., Lin, B., Ning, M., Yan, Y., Cui, J., Wang, H., Pang, Y., Jiang, W., Zhang, J., Li, Z., Zhang, W., Li, Z., Liu, W., and Yuan, L. Languagebind: Extending video-language pretraining to n-modality by language-based semantic alignment. In *International Conference on Learning Representations*, 2024. URL <https://arxiv.org/abs/2310.01852>.

A. Experimental Details

A.1. Model Checkpoints

We use the pretrained VLM models Qwen2.5-VL-7B-Instruct and Qwen3-VL-8B-Instruct, available at <https://huggingface.co/Qwen/Qwen2.5-VL-7B-Instruct> and <https://huggingface.co/Qwen/Qwen3-VL-8B-Instruct>, respectively. For the image super-resolution model, we use the pretrained checkpoint of DiT4SR available at <https://github.com/Adam-duan/DiT4SR>, specifically the ‘dit4sr.q’ checkpoint that was used in the original paper. For the video super-resolution model, we use the pretrained checkpoint of STAR at <https://github.com/NJU-PCALab/STAR>.

A.2. User Prompts

Image Super-Resolution. The user prompt used by the VLM during image super-resolution is as follows:

The second image is a low-resolution crop (bicubic upsample) of the first image.
 It may appear blurry due to upsampling, but you must ignore the blur.
 Compare both and describe the content of the SECOND image (the patch) with extreme detail.
 1. Intentional Texture: Based on the object’s identity, what is its actual material?
 2. Micro-OCR: Transcribe any letters, numbers, or symbols that are unique to this patch.
 3. Edge & Shape: Describe the intended sharp edges and structures of the objects in the patch.
 STRICT RULE: NEVER use words like ‘blurry’, ‘pixelated’, ‘noisy’, ‘low-res’, or ‘distorted’.
 Output ONLY the inferred high-quality keywords, separated by commas.

Video Super-Resolution. The user prompt used by the VLM during video super-resolution is as follows:

The second video is a low-resolution crop (bicubic upsampled) of the first video.
 It may appear blurry due to upsampling, but you must ignore the blur.
 Compare both and describe the content of the SECOND video (the patch) with extreme detail:
 1. Intentional Texture: Based on the object’s identity, what is its actual material?
 2. Micro-OCR: Transcribe any letters, numbers, or symbols that are unique to this patch.
 3. Edge & Shape: Describe the intended sharp edges and structures of the objects in the patch.
 STRICT RULE: NEVER use words like ‘blurry’, ‘pixelated’, ‘noisy’, ‘low-res’, or ‘distorted’.
 Output ONLY the inferred high-quality keywords, separated by commas.

B. Qualitative Examples of Prompt Misguidance

Semantic Interference in Global Prompts. In Section 4.1, we identified *prompt misguidance* as a critical issue where irrelevant semantic information in the global prompt perturbs the super-resolution process. Even when the global prompt c_{global} contains the correct keywords for a specific local patch, it is inherently coupled with descriptions of other regions. In the context of Classifier-Free Guidance (CFG), these irrelevant tokens are not merely ignored; they actively contribute to the conditioning vector e_{cond} . When the semantic content of the prompt conflicts with the visual evidence of the local patch (e.g., a global prompt describing “sky” and “buildings” applied to a patch containing only “pavement”), the model attempts to reconcile these conflicting signals. This results in *semantic interference*, where the model creates high-frequency artifacts or hallucinations attempting to manifest the irrelevant text descriptions.

Qualitative Examples. Fig. 6 illustrates this phenomenon in video super-resolution. We specifically show cases where the baseline fails to reconstruct accurate textures despite the global prompt including a correct description. We attribute this to the presence of nuisance descriptions that steer the generative trajectory away from its ideal direction. Thus, our Tiled Prompts method also acts as a semantic filter, providing a clean textual condition only containing relevant content. This is further supported by the quantitative results in Tab. 1 and Tab. 2 where our method achieves substantially higher alignment with text, such that the textual conditions provided are better aligned with the actual input visual content.

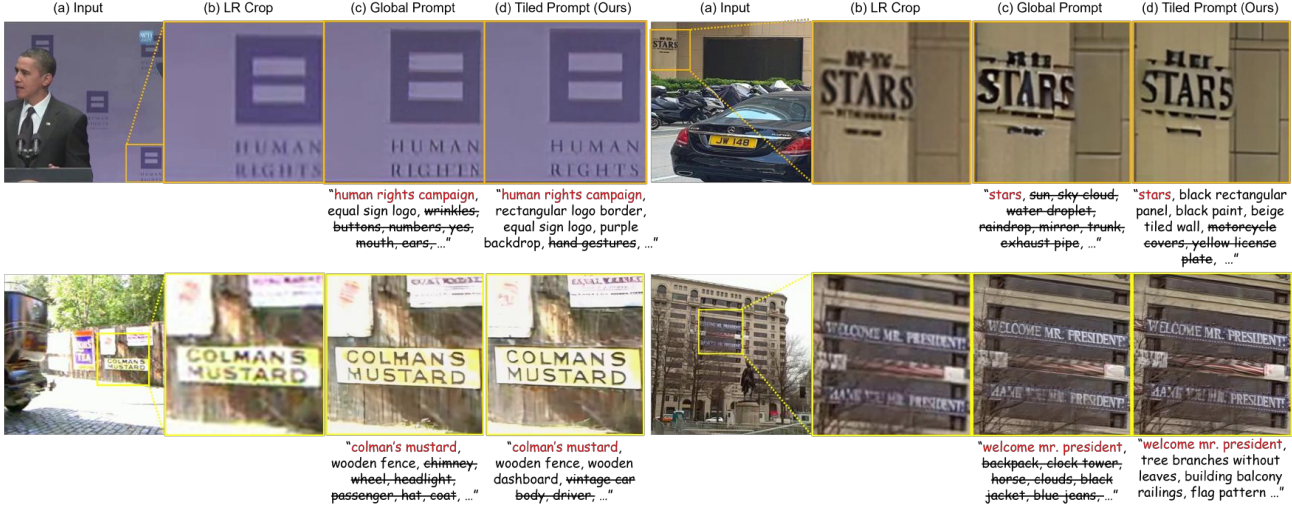


Figure 6. Examples of **prompt misguidance** in Video SR. **(a,b) Input:** A low-resolution input frame and its cropped tile. **(c) SR with Global Prompt:** The global prompt correctly mentions the target object (e.g., “human rights campaign”), but also introduces prompt misguidance by including descriptions of the surrounding scene (e.g., irrelevant prompts like “wrinkles”, “buttons”). This causes semantic interference, introducing artifacts and causing suboptimal reconstruction. **(d) SR with Tiled Prompt (Ours):** By filtering out these nuisance descriptions, our method provides a semantically clean textual condition, enabling the model to faithfully recover fine-grained details of the target structure.

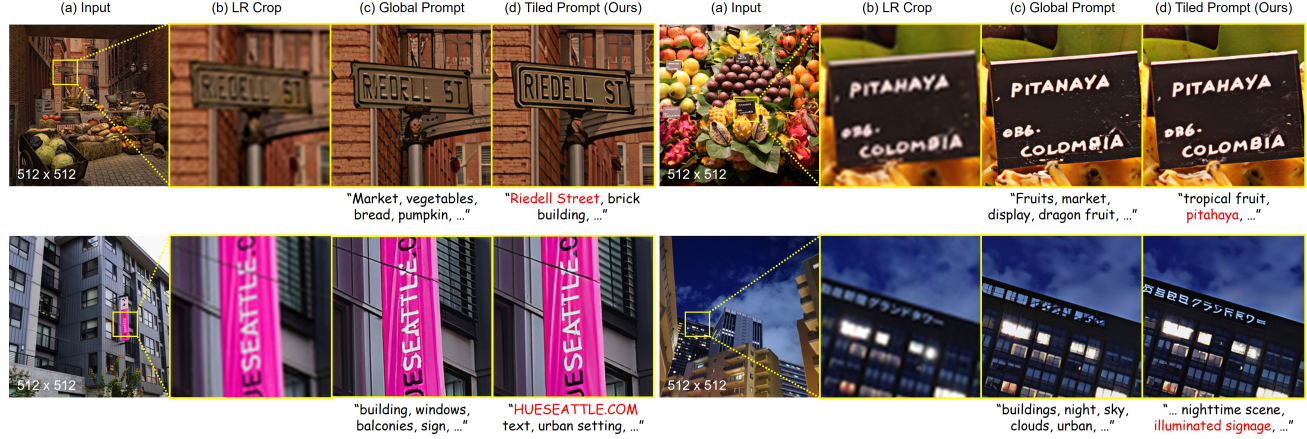


Figure 7. Additional qualitative results comparing **(a,b) the input image and its low-resolution crop**, **(c) SR results using the global prompt**, and **(d) SR results using the tiled prompt**.

C. Additional Qualitative Results

We provide additional qualitative comparisons in Fig. 7.